

Does a Fast Nuclear Magnetic Resonance Spectroscopy- and X-Ray Crystallography Hybrid Approach Provide Reliable Structural Information of Ligand-Protein Complexes? A Case Study of Metalloproteinases[†]

Johan Isaksson,^{*,‡} Susanne Nyström,[‡] Dean Derbyshire,[‡] Hans Wallberg,[‡] Tatiana Agback,[‡] Helena Kovacs,[§] Ivano Bertini,^{||,⊥} Andrea Giachetti,^{||,○} and Claudio Luchinat^{||,▽}

Medivir AB, PO Box 1086, SE-141 22 Huddinge, Sweden, Bruker BioSpin AG, Industriestrasse 26, CH-8117 Fällanden, Switzerland, Magnetic Resonance Center (CERM), University of Florence, Via Luigi Sacconi 6, 50019 Sesto Fiorentino, Italy, Department of Chemistry, University of Florence, Via della Lastruccia 3, 50019 Sesto Fiorentino, Italy, Department of Agricultural Biotechnology, University of Florence, Via Maragliano 75–77, 50144 Florence, Italy, ProtEra S.r.l., Via delle Idee 22, 50019 Sesto Fiorentino, Italy

Received November 3, 2008

A human matrix metalloproteinase (MMP) hydroxamic acid inhibitor (CGS27023A) was cross-docked into 15 MMP-12, MMP-13, MMP-9, and MMP-1 cocrystal structures. The aim was to validate a fast protocol for ligand binding conformation elucidation and to probe the feasibility of using inhibitor–protein NMR contacts to dock an inhibitor into related MMP crystal structures. Such an approach avoids full NMR structure elucidation, saving both spectrometer- and analysis time. We report here that for the studied MMPs, one can obtain docking results well within 1 Å compared to the corresponding reference X-ray structure, using backbone amide contacts only. From the perspective of the pharmaceutical industry, these results are relevant for the binding studies of inhibitor series to a common target and have the potential advantage of obtaining information on protein–inhibitor complexes that are difficult to crystallize.

Introduction

Accurate and time efficient structural information on ligand–protein complexes is of key importance for rational drug design in the pharmaceutical industry. Two methods are regularly used to solve high resolution ligand–protein structures: X-ray crystallography and nuclear magnetic resonance (NMR^α).¹ Of the two, X-ray is usually prioritized over the NMR technique despite the fact that the latter provides information of both structure and dynamics *in solution*. This is due to the fact that a full structure elucidation of the inhibitor–protein complexes by NMR is a time-consuming multiple stage process.² In general, NMR is used in the cases when a diffracting crystal can not be obtained.

Both methods reliably produce “high resolution” modeled structures based on large experimental data sets, which have given enormous insight into biological function and mechanisms. However, when looking further into the fine molecular detail to distinguish for example the binding energies of two similar inhibitors with often nearly identical binding conformation, it has proven very challenging to explain differences in activity.³ The main complication in correlating the true ligand–protein complex nature (i.e., activity) to the acquired data is that the measured primary quantities are nonlinear time averages and

can equally likely be attributed to very different combinations of conformational distributions in a *n*-state model.^{4–6} For instance, from experimental NOE data, it is not possible to distinguish a one-state from a two-state or a *n*-state model in quick exchange.⁷ To further complicate the task, the degrees of freedom are typically much larger than the number of measured quantities.⁸ Both NMR and X-ray further rely on force field parametrization, and in X-ray crystallography, there is also the potential problem of the crystallization process that itself can act as a selection criteria for the studied states, making it even more difficult to deduce the significance of the produced structures. Effort is continuously put into further understanding and better correlating the dynamic nature of biomolecules to raw experimental data using unconstrained molecular dynamics simulations together with NMR^{4,6,9–13} and small-angle X-ray scattering^{14,15} with promising results, but there are still time limitations in terms of molecular system size, the length of the trajectory needed to catch the relevant motions, specific protein labeling, and the level of theory employed.

In the light of this, it becomes relevant to discuss how far one wants to pursue the detailed description of what can only be considered a “representative” structure of a protein–inhibitor complex where its fine details, regardless of resolution/quality, often hold little information that we can currently translate into a truly significant understanding of the overall *potency* of the inhibitor. The aim is to see what accuracy we can sacrifice without moving out of the resolution window of significance (i.e., losing significant interpretable information) in order to increase the time and cost efficiency of the NMR method in the pharmaceutical industry.

Bertini et al. had earlier proposed a docking protocol¹⁶ for high throughput ligand docking using ¹⁵N single labeled protein with known assignment and structure. The present work further expands and rationalizes the procedure of obtaining the binding conformation and orientation of an inhibitor in a protein target. Considering that the cost of ¹³C-labeled glucose is no longer

[†] The MMP-12 + CGS27023A X-ray structure coordinates have been deposited to the Protein Data Bank, accession code: 2W0D.

* To whom correspondence should be addressed. Phone: +46-8-546 832 27. Fax: +46-8-546 831 99. E-mail: johan.isaksson@medivir.se.

[‡] Medivir AB.

[§] Bruker BioSpin AG.

[⊥] Department of Chemistry, University of Florence.

^{||} Magnetic Resonance Center (CERM), University of Florence.

[▽] Department of Agricultural Biotechnology, University of Florence.

[○] ProtEra S.r.l.

^α Abbreviations: MMP, matrix metalloproteinase; NMR, nuclear magnetic resonance; rmsd, root-mean-square deviation; MD, molecular dynamics; NOESY, nuclear Overhauser effect spectroscopy; NOE, nuclear Overhauser effect; HSQC, heteronuclear single quantum coherence; COSY, correlation spectroscopy; TOCSY, total correlation spectroscopy.

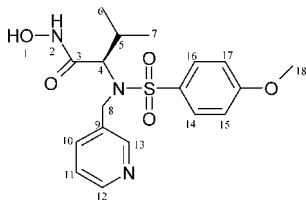


Figure 1. The chemical structure of the hydroxamic acid inhibitor **1**.

prohibitive compared to the work it can save and the fresh possibilities of X-filtered experiments, we have based our work on uniformly double labeled ($^{15}\text{N}/^{13}\text{C}$) protein and unlabeled inhibitor. This allows not only quick assignment of the protein backbone of the free protein as well as that of the protein–inhibitor complex but also the acquisition of X-filtered inhibitor to protein transfer experiments on the same sample.

MMP-12 in complex with a hydroxamic acid inhibitor, **1** (CGS27023A, Figure 1)¹⁷ was selected as a reference sample and has been studied by both X-ray crystallography and NMR to obtain complementary information. By adopting this strategy, the accuracy of the developed NMR-based docking procedure could be evaluated. It is interesting as a model system because it is biologically relevant and the whole family has a structurally conserved active site but with a somewhat different binding (specificity) pocket.

In short, matrix metalloproteinases (MMPs) are zinc-dependent endopeptidases involved in the degradation of connective tissue matrix proteins both in normal tissue turnover and in pathological tissue damage. Depending on substrate specificity, amino acid similarity, and identifiable sequence motifs, the family of MMPs can be loosely classified into distinct subclasses, some of which are: collagenases (MMP-1, MMP-8, and MMP-13), gelatinases (MMP-2 and MMP-9), stromelysins (MMP-3, MMP-10, and MMP-11), matrilysin (MMP-7), and metalloelastase (MMP-12).^{18–20} MMP-12 (also known as human macrophage elastase) plays an important role in the migration of monocytes/macrophages through the basement membrane²¹ and in the destruction of elastin in the lung alveolar wall.²² MMP-12 is of interest as a drug target, as it is believed to be involved in many diseases, such as chronic obstructive pulmonary disease, rheumatoid arthritis, and multiple sclerosis.^{23–25} The structure of the catalytic domain is globular and comprises a five-stranded β -sheet, three α -helices, and several extended loops. The catalytic zinc ion is coordinated by three extended histidine residues from the sequence motif HExxHxxGxxH, and the protein fold is stabilized by an additional structural zinc ion as well as by three calcium ions. These additional ions rigidify otherwise unstable loops and “zip” secondary elements together: loop $\beta 1/\alpha 1$ links to loop $\beta 5/\alpha 2$, the $\beta 2/\beta 3$ loop with the $\beta 4/\beta 5$ loop, loop $\beta 2/\beta 3$ links to both $\beta 4$ and $\beta 5$, and finally the $\beta 3/\beta 4$ loop links with $\beta 5$.

This study was designed to explore under which conditions protein–ligand studies by NMR can be performed in a time/cost-effective manner in the pharmaceutical industry. Hence, focus is on determining the ligand binding structure from NMR data at an early drug development stage to complement X-ray crystallography when diffracting crystals are not available.

Methods

Synthesis. The hydroxamic acid inhibitor, (**1**), was synthesized according to the method of MacPherson et al.¹⁷

Protein Cloning, Expression, and Purification. The catalytic domain of human MMP-12, corresponding to G106–G263, was

cloned into the expression vector pET11a. The mutation F171D was made to improve protein solubility²⁶ for NMR experiments. A second construct with the additional inactivating mutation E219A was engineered for long-term stability.²⁷ A third construct, comprising the inactivating mutation but lacking the F171D mutation, was produced for completeness. This last form was subsequently used in crystallographic experiments. Uniformly $^{15}\text{N}/^{13}\text{C}$ -labeled MMP-12 was produced in *Escherichia coli* BL21(DE3) grown in a defined medium²⁸ with 0.5 g/L of ^{15}N - NH_4Cl and 2 g/L of ^{13}C -D-glucose as nitrogen and carbon sources, respectively. For expression and purification, essentially the procedure by Morales et al.²⁹ was followed.

NMR Sample Preparation. The purified $^{15}\text{N}/^{13}\text{C}$ -labeled MMP-12 NMR sample was prepared by buffer exchange into an NMR-buffer containing 10 mM deuterated TRIS-HCl, pH 7.0, 100 mM NaCl, 5 mM CaCl_2 , 0.1 mM ZnCl_2 , 2 mM NaN_3 , and 10 mM deuterated DTT in 90% $\text{H}_2\text{O}/10\%$ D_2O . Buffer exchange was carried out on prepacked PD-10 column (Sephadex G-25; GE Healthcare, Sweden). The sample was concentrated to 0.7 mM in a Vivaspin 15R centrifugal filter unit (VivaScience, Germany). In experiments with inhibitor, this was added in a 2:1 ratio (inhibitor: enzyme). Care was taken not to exceed 5% DMSO in the NMR samples.

Crystallization and X-ray Structure Analysis. The MMP-12+(**1**) complex was crystallized using the “hanging-drop” vapor diffusion method,³⁰ resulting in a refined structure at approximately 2.0 Å resolution. The crystallization protocol is described in further detail in the Supporting Information.

NMR Data Collection. All experiments were part of the standard Bruker TopSpin 2.1 pulse program package and were performed at 22 °C, using Bruker Avance II spectrometers operating at 500, 600, 700, and 900 MHz ^1H -frequency, equipped with cryogenically cooled inverse triple resonance probes. For more details, see the Supporting Information.

NMR Signal Assignment. The protein backbone-connected N, CA, CB, CO, HN, HA, and HB resonances were fully assigned using a combination of the standard protein experiments HNCA, HN(CO)CA, HNCACB, HNCO, HN(CA)CO, HBHANH, and HBHA(CO)NH. The more peripheral aliphatic side chain resonances were assigned using (H)CCH- and HC(C)H-type COSY and TOCSY spectra.

The signal assignment and integration was straightforward and was performed using the software CARA, version 1.5.3.³¹

Interproton Distance Restraints. The ligand-proton NOE-contacts were extracted from the linear build-up region of ω_2 - ^{15}N -edited/ ω_1 - ^{15}N , ^{13}C -filtered (^{15}N -X-filtered), and ω_2 - ^{13}C -edited/ ω_1 - ^{15}N , ^{13}C -filtered (^{13}C -X-filtered) NOESY spectra (at 75 ms mixing time). Because of the absence of any straightforward reference distances in the X-filtered experiments, the contacts were classified in three categories: strong (3.0 Å), medium (4.0 Å), and weak (5.0 Å). The resulting restraint list was then modified according to the following set of rules for different types of interaction.

(1) 0.5 Å was added to the ambiguous isochronous contacts of phenyl side chain protons to compensate for the uncertainty in the NOE-contact (because it is unknown whether only one or both of the two protons contribute to the NOE intensity in the most populated rotation angles of the ring).

(2) 1.5 Å was added to all methyl interactions and the restraint point was moved to the methyl carbon.

(3) 2.5 Å was added to all O-methyl interactions to allow for the quick rotation of this group that enables it to collect NOE cross peak intensity over a large surface.

Trial calculations performed using integrated restraints based on arbitrary reference distances slightly reduced the accuracy of the docking calculations and added more NOE strain (Table S2 in the Supporting Information). Relaxation of these restraints led to a further reduction in the accuracy of the docking.

Computation. Ligand Generation. The ligand was generated by starting from the MMP-12+(**1**) X-ray complex, hydrogens were added, and the structure was minimized using semiempirical calculations (AM1 type Gaussian 98).³² Parameters and topology

Table 1. Classification of the Assigned nOe Contacts between **1** and MMP-12

	H(¹⁵ N)	H(¹³ C)
strong	4	2
medium	10	10
weak	8	6

were generated using the Xplo2D³³ program, and all dihedral angles energy constants were set to zero. Only dihedral angles required for ring planarity and maintenance of correct stereochemistry were set to an energy constant value of 750.0 kcal·mol⁻¹·rad⁻². Finally, Gasteiger–Marseli charges³⁴ were assigned using the OPENBABEL³⁵ program.

Autodock. An identical set of Autodock parameters to the one described in previous MMP-12 work by Bertini et al.¹⁶ was used to generate starting structures of the ligand inside the active site. In brief, a grid box of 70 Å × 70 Å × 70 Å was centered on the active site (the residue cluster displaying chemical shift perturbation upon inhibitor addition) with a grid spacing of 0.375 Å. Crossover-, mutation-, and elitism weights were set to 0.80, 0.02, and 1.0, respectively. 100 docking calculations were made for every crystal structure. These were clustered within 1 Å rmsd and evaluated according to the lowest docking energy.

Xplor-NIH. A modified simulated annealing protocol was used to apply the NOE distance restraints and minimize the ligand energy. All molecular dynamics were performed on a fully rigid (grouped) protein in vacuo using CHARMM nonbonded parameters.³⁶ The system was first heated to 1000 K during 2.4 ps and then cooled down to 50 K during 6 ps, followed by 1000 steps of Powell minimization. The NOE-restraints were scaled to 5, 2, and 1 kcal mol⁻¹ Å⁻² for the strong, medium, and weak NOE restraints, respectively (Table 1). Using steeper energy penalties for NOE violations did not increase the accuracy compared to the reference X-ray structure (data not shown). During the whole simulation, the force field energy terms for angles, bonds, dihedrals, electrostatics, van der Waals, and impropers were also active. In addition, a planarity restraint was applied to the zinc binding during the minimization. Only energy contributions from the protein residues near the ligand binding site were included in the reported total energy in order to reduce the background energy from the locked protein residues far from the site of interaction. Representative structures from each of the three lowest energy clusters of Autodock conformations were used as starting structures to create 100 XPLOR-NIH minimized structures for each, resulting in a total of 300 dockings per protein–ligand combination.

Root-Mean-Square Deviation. The rmsd values were calculated using a slightly modified version of the standard XPLOR-NIH protocol rmsd.inp. First the backbone atoms of the active site (residues 180–186, 213–220, and 238–243) were used to fit the MMPs to the reference crystal structure of MMP-12+(**1**) and the rmsd's for the different X-ray structures are reported in Table 2. Without further fitting, the rmsd was then measured between the heavy atoms of the docked ligand in the MMPs and the position of the ligand in the reference crystal structure. The pyridine ring was excluded from the rmsd calculations because it is completely unconstrained and extrudes from the active site so that its orientation is determined by the Xplor-NIH force field.

Results and Discussion

Our reference sample, MMP-12+(**1**), was studied by both X-ray crystallography and NMR spectroscopy to obtain complementary information to allow us estimate the accuracy of our NMR-based docking procedure.

The first section complements the methodology previously described by Bertini et al. with the deployment of X-filtered experiments. This permits a faster and more precise definition of the inhibitor binding conformation.

In the second section, the inhibitor is docked into several MMP-12 structures. Because solution data is used to dock the

inhibitor, **1**, into a solid-state static protein structure, it is relevant to dock it into an ensemble of X-ray structures to better mimic the structural heterogeneity expected in solution.³⁷

The procedure is then challenged in the third section by docking the inhibitor, **1**, into MMP-9, MMP-13, and MMP-1 with the aim of finding the lower limit of homology that is required to return a relevant binding conformation.

X-Ray Structure Analysis. The MMP-12 cocrystal structure with **1** (submitted to the Protein Data Bank, accession code 2W0D, referred to as “ref” in this work), generated for the purpose of the present analysis, has essentially the same conformation as the one previously reported by Nar et al.³⁸ (Protein Data Bank, accession code 1JIZ). This previously published structure represented a complex with the active form of MMP-12. The two construct differences, the E216A mutation in the active site and a shortening of both termini (by 7 and 1 residue[s] at the N- and C-terminus respectively), did not result in any major changes to the overall structure. Indeed, the only structural difference of note was restricted to a segment of the “extended” S1' cavity (specifically residues 246–248).

The glutamate to alanine switch in the active site (the E216A mutation) did not crucially affect the conformation of the active site nor of the bound compound. However, crystal packing does lead to a movement of the pyridyl ring, allowing the same ring group from a neighboring molecule to stack. The latest example of MMP-12 being used here displays the same protein fold reported for the MMP Zn-protease protein family as a whole (Figure 2).

The crystal structure suggests that **1** binds with both hydroxamate oxygen atoms coordinating the zinc ion, and the hydroxamate amino group forms a hydrogen bond to the main-chain carbonyl of residue A182. The only other hydrogen bond found is from one of the sulfone oxygen atoms to the main-chain NH of L181. This is in good agreement with the published “active-enzyme” structure (1JIZ³⁸), although in the latter there is an additional hydrogen bond between a hydroxamate oxygen and the active site glutamate side chain. Neither the isopropyl substituent nor the pyridyl ring of the remaining ligand groups is involved in any direct interaction with the enzyme, both being mainly solvent-exposed. Only the methoxyphenyl moiety in the S1'-pocket gives any additional contribution to the binding affinity via hydrophobic packing and it may include a weak “aromatic” interaction with H218.

NMR Analysis. X-filtered ligand–ligand NOESY and TOCSY spectra of the MMP-12+(**1**) sample were used to assign the ligand resonances in the bound conformation (Figure 3). In the case of MMP-12, the structural data of the bound ligand is, however, limited. The only conformationally relevant NOE was the intraligand HN2 to H4 cross peak (green box, Figure 3) that positions these two atoms on the same side of the molecule frame. This type of observation can be very useful when studying more rigid inhibitors like macrocycles where the information could be used to exclude false theoretical docking results.

Interestingly, the spectrum reveals several features about the dynamics of the bound ligand. As previously reported⁴⁰ for **1** in stromelysin (MMP-3), the two methoxy-phenyl ortho- and meta-protons both have isochronous chemical shifts, which indicates that the ring can rotate faster than the millisecond scale. A similar but less straightforward observation is made for the pyridine ring. There is no single ring orientation where both the ortho-protons (H10 and H13) can simultaneously show cross peaks of roughly equal intensities to HM7, H5, H8' and H8'' protons. One can conclude that the pyridine moiety is also

Table 2. Summary of the Selected X-ray Structures Used in the Dockings^a

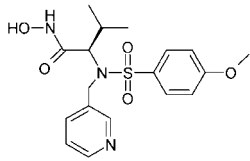
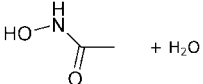
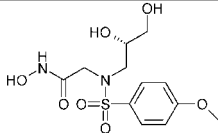
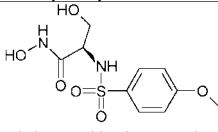
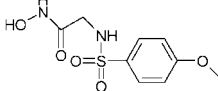
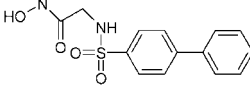
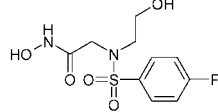
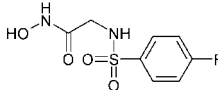
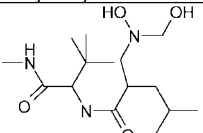
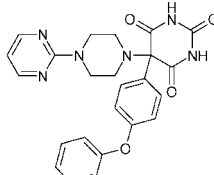
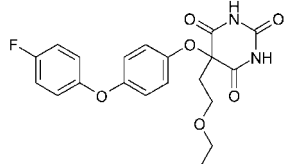
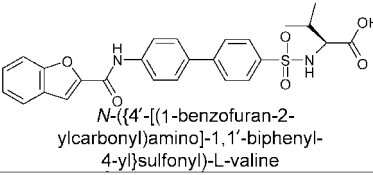
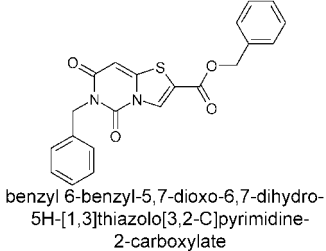
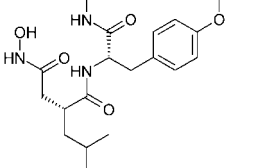
Protein	ID	Res. (Å)	Ligand	Active site RMSD (Å)	Identity
MMP-12	Ref ^a	2.00	 1	-	100%
MMP-12	1Y93 ⁴³	1.03	 + H ₂ O acetohydroxamic acid	0.42	99.0%
MMP-12	Diolo ^a	1.70	 (S)-2-(N-(2,3-dihydroxypropyl)-4-methoxyphenylsulfonamido)-N-hydroxyacetamide	0.32	99.0%
MMP-12	Eat018 ^a	1.16	 (R)-N,3-dihydroxy-2-(4-methoxyphenylsulfonamido) propanamide	0.34	99.0%
MMP-12	Mlc148 ^a	1.25	 N-hydroxy-2-(phenylsulfonamido)acetamide	0.35	99.0%
MMP-12	Mlc73 ^a	1.10	 2-(biphenyl-4-ylsulfonamido)-N-hydroxyacetamide	0.30	99.0%
MMP-12	Mlc94 ^a	1.13	 2-(4-fluoro-N-(2-hydroxyethyl)phenylsulfonamido)-N-hydroxyacetamide	0.33	99.0%
MMP-12	Mlc99 ^a	1.13	 2-(4-fluorophenylsulfonamido)-N-hydroxyacetamide	0.32	99.0%
MMP-9	1GKC ⁴⁴	2.3	 2-amino-N,3,3-trimethylbutanamide	0.40	55.9%
MMP-9	2OVX ⁴⁵	2.0	 5-(4-phenoxyphenyl)-5-(4-pyrimidin-2-ylpiperazin-1-yl)pyrimidine-2,4,6(2H,3H)-trione	0.21	55.9%

Table 2. Continued

Protein	ID	Res. (Å)	Ligand	Active site RMSD (Å)	Identity
MMP-9	MID134937	2.0	<i>n.a.</i> ^a	0.29	55.9%
MMP-13	1YOU ⁴⁶	2.3	 5-(2-ethoxyethyl)-5-[4-(4-fluorophenoxy)phenoxy]pyrimidine-2,4,6(1H,3H,5H)-trione	0.53	61.7%
MMP-13	1ZTQ ⁴⁷	2.0	 <i>N</i> -({4'-[(1-benzofuran-2-ylcarbonyl)amino]-1,1'-biphenyl-4-yl}sulfonyl)-L-valine	0.60	61.9%
MMP-13	2OW9 ⁴⁸	1.74	 benzyl 6-benzyl-5,7-dioxo-6,7-dihydro-5H-[1,3]thiazolo[3,2- <i>C</i>]pyrimidine-2-carboxylate	0.58	61.9%
MMP-1	1FBL ⁴⁹	2.50	 <i>N</i> -[3-(<i>N'</i> -hydroxycarboxamido)-2-(2-methylpropyl)-propanoyl]-O-tyrosine- <i>N</i> -methylamide	0.48	62.6%

^a Some properties of the crystal structures are included: crystal diffraction resolution, the sequence identity to the reference crystal, and the rmsd of the heavy atoms of the active sites between the crystal structures and the reference structure. #: Undisclosed proprietary compound within the scope of international patent application no WO 07/68474 and representing an additional data point following the overall trend. *: Not published.

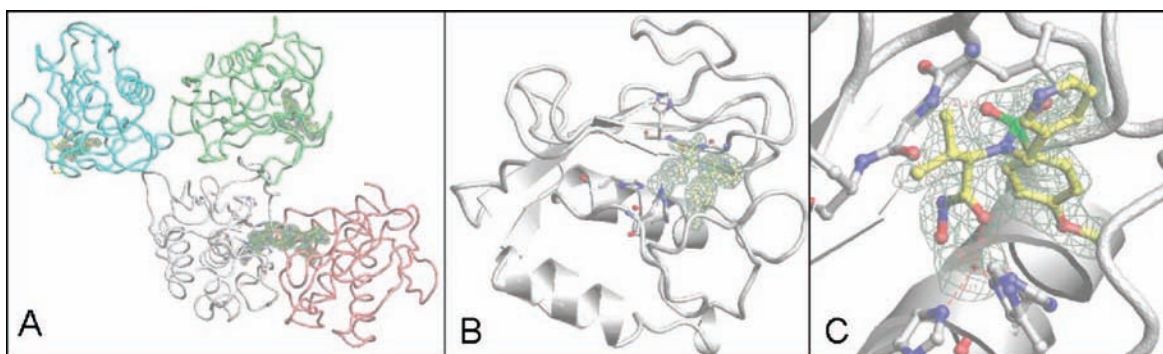


Figure 2. X-ray structure of MMP-12 inactivated mutant in complex with the hydroxamate inhibitor **1**. (A) Four molecules of the asymmetric unit, (B) enlargement of a single molecule, and (C) close-up of the active site interactions. Figures produced from screen captures of O³⁹ in each case show the electron density ($2f_o - f_c$ contoured at 1σ) for the inhibitor.

rapidly changing orientation in the bound state, although the asymmetric heterosubstitution of the ring prevents the two ortho-protons from being magnetically equivalent. The IC₅₀ of ~2.0 nM for MMP-12+(**1**) implies that these rotations do not require complete inhibitor disassociation but are taking place in the bound state.³⁸

The above observations confirm the existence of significant internal dynamics of the inhibitor and provide valuable insight into what parts of the molecule have a less defined bound conformation. With this information available at an early stage, it is possible to make a well-founded decision whether to pursue a high resolution structure on this system or to use a reliable

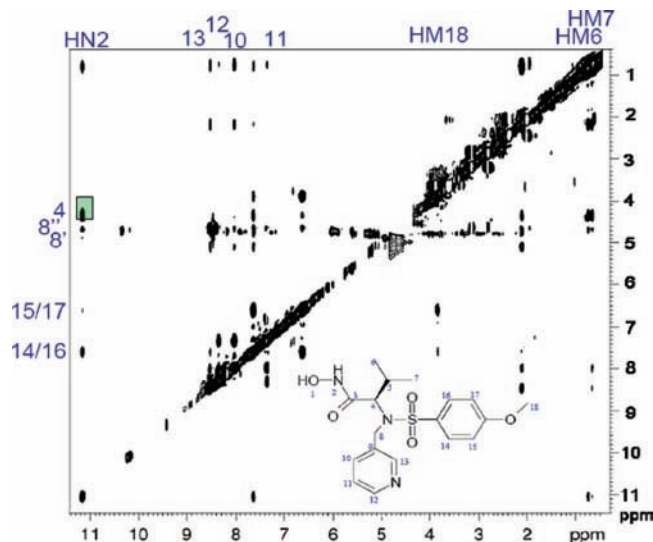


Figure 3. X-filtered NOESY showing the natural abundance inhibitor–inhibitor NOEs. This type of spectra permits a quick assignment of the studied inhibitor in its bound state. The structurally relevant HN2–H4 NOE is highlighted in green.

but more approximate approach to obtain a starting point for a more thorough dynamics analysis. Although it is highly desirable, obtaining a full understanding of the internal dynamics is presently a too complex and time demanding process for the scope of this work. This is however an area of extensive research^{4,6,8–12} that needs to be monitored closely in the future as to when these methodologies become viable for routine use.

NMR Assignment. The backbone was fully assigned for residues 108–121, 125–167, and 172–261. Absence of connectivity prevented full assignment of the gaps belonging to two of the loops and the terminals (Figure 4). Only a few of the aliphatic side chain resonances could not be assigned because of spectral overlap or lack of signal, whereas we did not succeed in connecting the rings of the aromatic side chains to their backbone positions.

Ligand–Protein Contacts. Initially, a series of 2D ^1H – ^1H planes of the 3D ^{13}C -X-filtered NOESY were recorded with mixing times of 25, 50, 75, 100, 125, and 150 ms. In Figure 5, the signal intensities of five arbitrarily chosen intermolecular cross peaks are plotted as a function of the mixing time. The linear regime of the NOE build-up rate, where the two-spin approximation is still valid, appears to extend roughly up to 100 ms mixing time. Thereafter, the competing effects hamper the proportionality between the intensities and the internuclear distances. Moreover, a number of new cross peaks appear in the spectra obtained with 125 and 150 ms mixing times, indicating that spin diffusion effectively spreads the magnetization to neighboring spins. On this basis, signal intensities for conformational restraints were analyzed from the 3D X-filtered NOESY experiments recorded with a mixing time of 75 ms.

The ^{15}N - and ^{13}C -X-filtered 3D NOESY spectra were recorded at four field strengths, 500, 600, 700, and 900 MHz. Scrupulous comparisons of these spectra revealed no substantial differences in the detectable NOE cross peaks. The spectra at 600 MHz recorded with a mixing time of 75 ms allowed us to extract a total of 22 $\text{H}(^{15}\text{N})$ contacts and 18 $\text{H}(^{13}\text{C})$ contacts to the ligand. The ^1H – ^1H planes from the ^{15}N 3D NOESY spectrum are displayed in Figure 6.

The NOE cross peaks were then classified as strong, medium, or weak and assigned an upper bound of 3, 4, and 5 Å, respectively, and subsequently modified according to the rules

described in the Methods section. The distribution of the NOE contacts is illustrated in Figure 7, and the classification of the NOE restraints is reported in Table 1. Among the $\text{H}(^{13}\text{C})$ contacts, 11 were to protein methyl groups, six to methylene protons, and one to a CH-group. Four NOE cross peaks at aromatic frequencies of the protein were discarded because the missing assignment of the aromatic side chains. In total, four contacts from the ligand to unassigned aromatic side chains were found that should be compared to the maximum of six theoretical contacts nearer than 5 Å between aromatic side chain protons and ligand atoms in the reference X-ray structure. These contacts were not considered to add any accuracy to the calculations because they were relatively few and the interaction points on the ligand all belonged to the rotationally ambiguous methoxyphenyl protons. They were thus not pursued further. In addition to the ligand-specific contacts, some protons not belonging to the ligand show both $\text{H}(^{15}\text{N})$ and $\text{H}(^{13}\text{C})$ contacts. These contacts have been found to arise from glycerol artifacts from the protein filtration in the sample preparation (data not shown).

Computer Modeling of the MMP-12+(1) Complex. To test whether a more time efficient procedure can be achieved, we did not aim to solve the protein structure for this type of docking but instead docked the ligand in available X-ray structures. The correlation between raw data, NMR-, and X-ray structures is under constant debate, and lately there has seemed to be a consensus that no individual structure fully represents the native state of the protein. Instead, an ensemble of structures solved under different conditions and/or different sequence homology give a representation of the native state heterogeneity.⁵ For this reason, it makes sense to use a structure as similar as possible to the studied target as it is likely to reside somewhere inside the hyperspace representative of the natural state of the protein. We aim at demonstrating that if one can accept the above approximation one can cut the time required for the docking calculation to less than a quarter compared to a full structure elucidation by NMR, which is considerably time-consuming.

First, serving as a point of reference, the NMR derived distance restraints were used to redock the inhibitor, **1**, into the X-ray structure of the same sample (MMP-12+(1)) where the inhibitor had been cut out. The program Autodock 3.05⁴¹ was used throughout. The three lowest energy Autodock clusters placed the ligand at an rmsd of 1.22, 0.76, and 1.62 Å compared to the ligand position in the X-ray structure, respectively. This shows that Autodock by itself is a very time-efficient way to produce relevant starting structures when validation of the binding mode by experimental data is not imperative. After a cycle of NMR restrained Xplor-NIH MD, the average rmsd of the ligand decreased to 0.45, 0.45, and 0.59 Å, respectively, when using only the ligand–HN contacts and to 0.43, 0.43, and 0.57 Å, respectively, when using the ligand–HN contacts together with the ligand–HC contacts. Hence, for all three starting structures provided by Autodock, one cycle of NMR restrained MD brings the inhibitor to a position that lies significantly closer to the X-ray conformation than the starting point. This is interesting to note because in this X-ray structure the protein has been cocrystallized together with this very ligand and therefore the active site should by all means be a perfect imprint of the molecule to be docked into without using experimental input. Even so, the sum of all NOE restraints applied during a single MD cycle (which are time averaged and roughly classified) gives a structure closer to the X-ray structure compared to the theoretical docking (Figure 8, denoted “ref”).

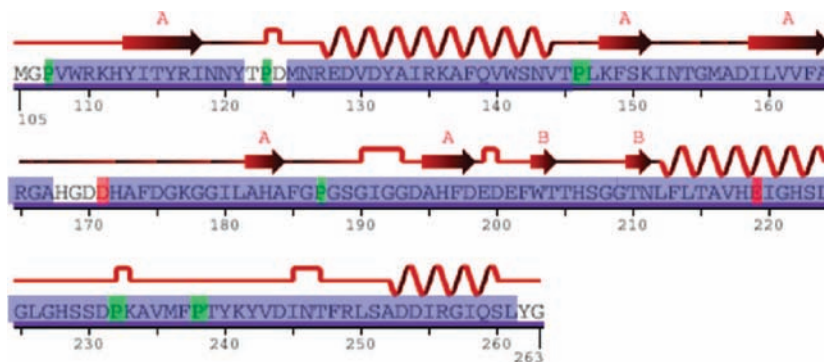


Figure 4. Schematic representation of the backbone assignment. Assigned residues are shaded blue, prolines are highlighted green, and the two sites of mutation are highlighted in red (F171D and E219A).

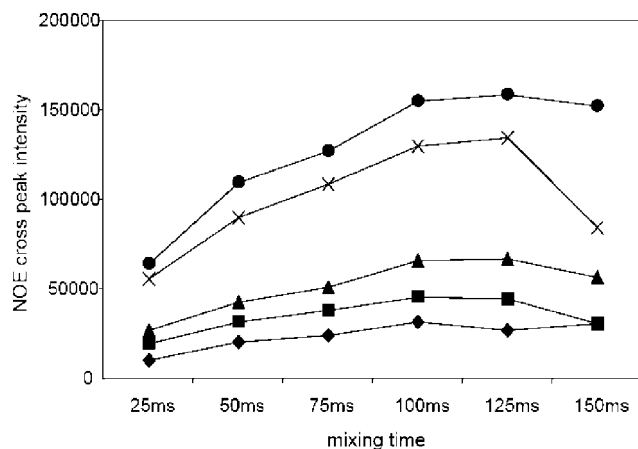


Figure 5. Signal intensity of five randomly selected intermolecular cross peaks depicted as a function of the NOESY mixing time. The signal intensities were extracted from 2D ^1H – ^1H planes of the 3D ^{13}C -X-filtered NOESY recorded at 600 MHz for 4 h each.

Further, the rmsd evaluation in Figure 8 shows that applying the HC contacts does not significantly improve the accuracy of the protocol compared to using the HN contacts alone. This is important because carbon assignment of protein side chains is considerably time-consuming with respect to both NMR time and person-hours. While this finding is likely to be system dependent, certainly for the MMPs of the current study we see no good reason to pursue the carbon data collection in order to improve the ligand binding conformation.

In the pharmaceutical industry, it is common to have access to both NMR and X-ray techniques, and in that context, the kind of docking described above is only interesting when (a) a series of inhibitors against the same target is analyzed and one wants to quickly confirm the binding mode without waiting for crystallization, and (b) when the protein target does not yield diffracting crystals. To test these scenarios, we have docked the inhibitor, **1**, in 15 different X-ray structures (Table 2) of MMPs as docking hosts to probe the effect of using ligand–protein interaction data on crystal structures that are related (but not identical) to the studied system. First, the in-house X-ray structure of the studied system, MMP-12+(**1**) (see X-Ray Structure Analysis Section), was selected to probe the accuracy under the approximation that the X-ray binding conformation is identical to one in solution. Second, seven structures of MMP-12s cocrystallized with different inhibitors were chosen to probe the impact of the ligand on the active site conformation (ID: 1Y93, Diolo, Eat018, Mlc148, Mlc73, Mlc94, and Mlc99). Finally, three MMP-13s (collagenases, ID: 1GKC, 2OVX, and MID134937), 3 MMP-9s (gelatinases, ID: 1YOU, 1ZTQ, and

2OW9) and one MMP-1 (interstitial collagenase, ID: 1FBL) structures were selected to test whether the method is at all applicable in cases where the only option is to use a different protein belonging to another class within the same protein family because the studied protein does not form crystals. The MMP-12 sequence identity to MMP-9, MMP-13, and MMP-1 is approximately 56%, 62%, and 63%, respectively, and the rmsd between the backbone atoms in the active sites are ~ 0.20 – 0.40 Å for the MMP-9s, ~ 0.55 – 0.60 Å for the MMP-13s, and 0.48 Å for the MMP-1 structure. The ligand of each structure and any active site water molecules were removed to make room for **1** in the active site. Autodock⁴¹ was used to generate low energy structures of the ligand **1**^{38,40} docked in the empty active sites of the selected X-ray structures and clustered within 1.0 Å. The three clusters with the lowest docking energies for each X-ray structure were used as starting structures in the molecular dynamics (MD) based minimizations in Xplor-NIH.⁴²

A distance restrained temperature cycling/MD protocol was used to generate 100 refined ligand conformations in the fixed protein X-ray structures for each of the Autodock generated ligand starting conformations using the NMR-derived distance restraints from the MMP-12+(**1**) sample.

The same docking experiment was repeated for all the selected crystal structures, and the resulting rmsd values are summarized in Figure 8. The superimposed structures are presented in Figure 9.

For five out of eight MMP-12 crystal structures (ref, 1Y93, Diolo, mlc73, mlc99), the lowest energy docking is within 0.5 Å of the X-ray structure. For the other three crystal structures (eat018, mlc94, and mlc148) the rmsd is within 1.1 Å.

For two out of three MMP-9 structures (1GKC, 2OVX), the lowest energy docking is within 0.7 Å and the third (MID134937) is within 1.2 Å.

For all MMP-13 structures (1YOU, 1ZTQ, 2OW9) and for the MMP-1 structure (1FBL), the lowest energy dockings is within 0.7 Å.

It is also noteworthy that for every single investigated structure, the NMR-restrained MD minimization yields structures that lie closer, and in several cases significantly closer, to the reference X-ray structure than the Autodock-generated structures. It could be argued that this is because the Autodock placement of the inhibitor with respect to the energy surface of the host protein is to a large extent dictated by the side chains, while the NMR restraints place the inhibitor mainly relative to the backbone, and it is thus only restricted by the side chains. However, the above observation is also valid for the reference X-ray structure where both the side chains and the backbone are optimized for inhibitor **1** itself by the crystallization process.

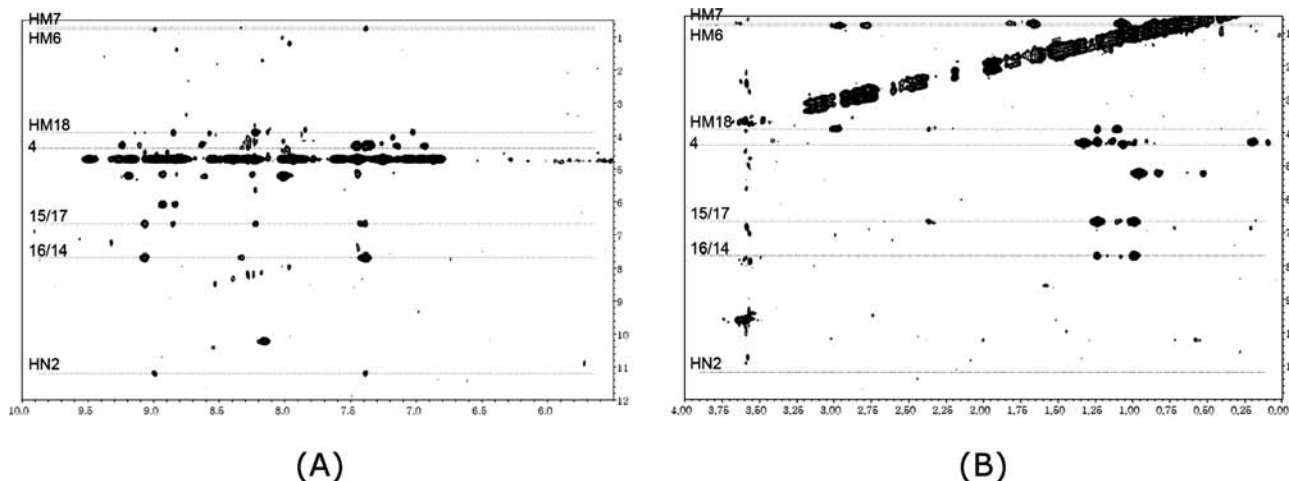


Figure 6. (A) ^{15}N -X-filtered 3D NOESY and (B) ^{13}C -X-filtered 3D NOESY showing the contacts from the natural abundance inhibitor to the $^{13}\text{C}/^{15}\text{N}$ labeled protein.

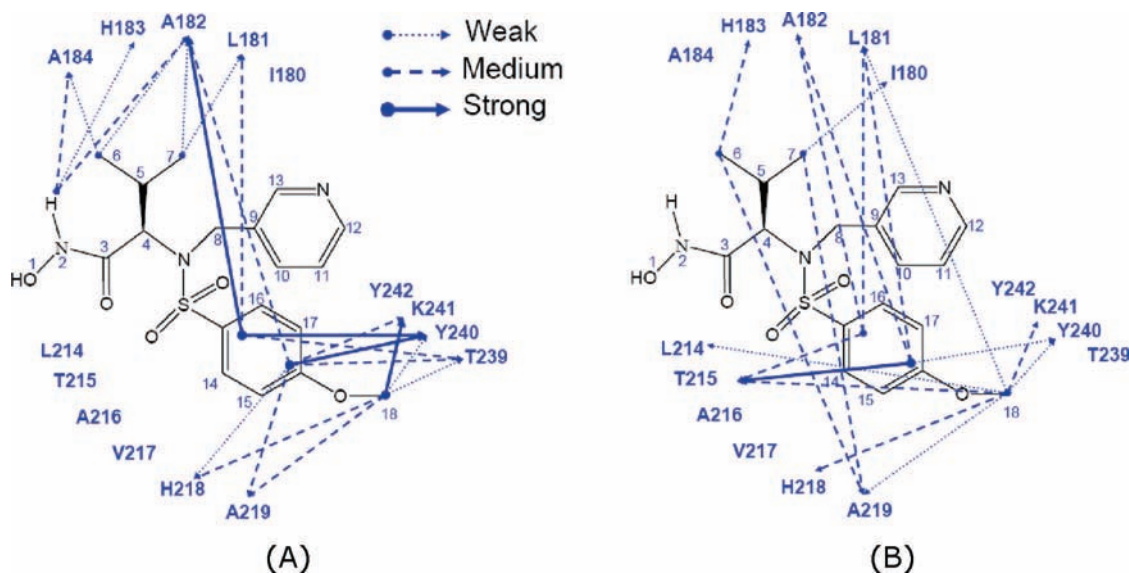


Figure 7. Chart of the protein–ligand contacts found at 75 ms mixing time showing (A) $\text{H}(^{15}\text{N})$ contacts and (B) $\text{H}(^{13}\text{C})$ contacts. Note that there are no contacts to the pyridine ring.

A final important observation concerning the rmsd/energy distribution is that one cannot reliably distinguish different minimized clusters after the restrained MD from each other if their rmsd to the reference structure is below ~ 1 Å in terms of docking energy. When the ligand drifts further than ~ 1 Å from the reference binding, the NOE energy terms respond accordingly. For this reason, it can be concluded that accuracy below ~ 1 Å can hardly be claimed from this data set. More detailed rmsd plots are provided in Figure S1 in the Supporting Information.

We conclude that the X-ray and NMR hybrid docking protocol discussed herein is a method to reliably and quickly identify the binding mode of an inhibitor. The rmsd of ~ 0.5 Å between the docked conformations and the X-ray reference conformation includes any intrinsic errors from the docking method, from the X-ray model refinement and from the difference between the time-averaged NMR data acquired in solution and the diffraction data acquired in crystalline state. In this respect, we consider these two inhibitor conformations equivalent.

The docking results in the ensemble of seven MMP-12 X-ray structures result in rmsd's between 0.5 and 1.1 Å (average 0.7

Å). This comparison reflects the most realistic application of the proposed method, where a potential drug candidate is docked into a homologous X-ray protein structure that has been cocrystallized with a different inhibitor. The variation in accuracy is to be expected and reflects the structural heterogeneity of the active sites of the structure ensemble. It is strongly recommended that an ensemble of structures is used in this application to reduce the impact of the cocrystallization effects of each individual protein structure and to reveal structural- or data inconsistencies and thereby provide some insight into the structural heterogeneity of the studied system.

The subsequent inclusion of seven protein structures from the MMP-1, MMP-9, and MMP-13 subclasses into the structural ensemble did not further reduce the accuracy of the docking calculations, the average rmsd remaining at 0.7 Å. Although mildly unexpected, it can be explained by the fact that the rmsd between the backbone atoms of the active sites between these structures and the reference structure are all below 0.6 Å, which can be masked by the estimated accuracy of these docking calculations toward the reference of about 1 Å.

We argue that the method described in this work is accurate enough to serve as starting point for more thorough analysis

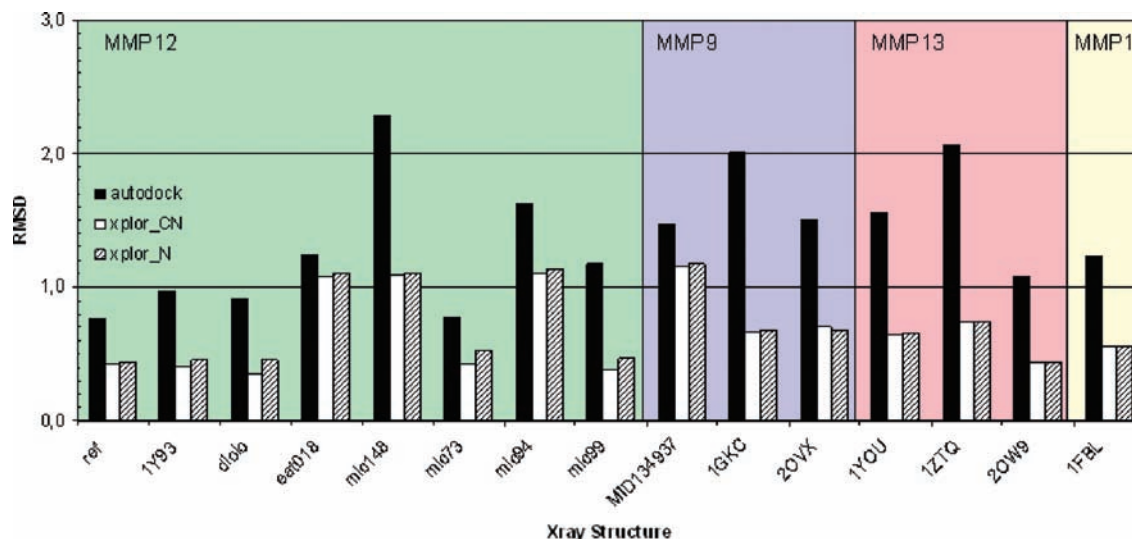


Figure 8. Summary of the average rmsd between **1** docked in various X-ray structures of MMPs and the reference X-ray structure of MMP-12+ (1). The solid bar is the rmsd for the unconstrained docking by Autodock, the hollow and slashed bars are the rmsd's after one cycle of NOE restrained X-PLOR minimization using either HC+HN restraints or only the HN restraints, respectively. The chart has been shaded with respect to which MMP family each protein belongs to. Here, only the lowest energy docking out of three is shown for each X-ray structure. For more details see the Supporting Information.

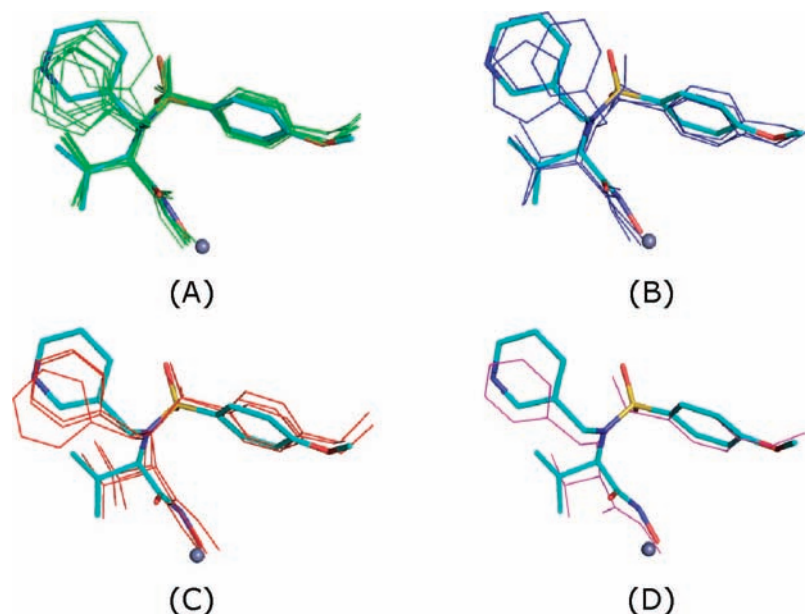


Figure 9. Superimpositions of the reference X-ray structure (2W0D) and the docking in (A) eight MMP-12 structures, (B) three MMP-9 structures, (C) three MMP-13 structures, and (D) one MMP-1 structure. In the figures, the heavy atoms in the backbones of the proteins have been fitted before the all protein atoms were stripped. The active site zinc is represented by a small sphere.

by thermodynamically calibrated molecular dynamics or high-dimensional QSAR. One can potentially use this approach to obtain some information about inhibitor binding when the target does not form crystals by docking into a related protein with known structure. The interpretation of the results becomes, however, more speculative. To apply data from one system onto another naturally requires caution as there are no direct means by which to validate the assumptions made. Indications of major conformational changes upon binding are most importantly the presence of significant line broadening or sharpening of a set of ^{15}N -HSQC peaks upon binding, especially if coupled to an alteration in chemical shift. If adaptive binding is observed, it is necessary to relax the protein with the inhibitor during the MD simulations, preferably in explicit water. In the current study, there were no indications of adaptive binding and with

back-calculated rmsd's below 0.5 \AA there was no reason to release the protein atoms and thereby introduce additional uncertainty.

We would like to stress that when designing potential drugs against a protein target where no structural data is available, any indices that promotes an educated guess can lead to a breakthrough. If the studied system is truly unknown, it is of great value to have a starting point backed up by experimental data that you can base subsequent unrestrained molecular dynamics simulations of the inhibitor–protein complex on.

It is also worth considering that the harder it is to produce diffracting crystals, the more likely the inhibitor is to be weakly bound (μM range) and the target protein to have flexible motif(s). Under these circumstances, the active site is expected to have a rather flat energy landscape for the inhibitor and would

likely be poorly described by a static picture even if one could be obtained by X-ray or a full NMR elucidation. As a result of this, the probability that the generated conformation reside within the hyperspace occupied by the inhibitor at biological temperatures is expected to increase and would hence serve as well as any other minimized structure within this hyperspace as a starting point for further characterization by computer simulations.

Acknowledgment. We thank Alexandra Johansson and Elisabet Lilja for excellent technical support with labelling and purification of the MMP-12 proteins. Support from the EU-NMR Integrated Infrastructure Initiative, contract no. RII3-026145, program for the use of the 900 MHz instrument at the CERM large-scale NMR facility in Florence, Italy, Ministero Italiano dell'Università e della Ricerca (MIUR), through the FIRB projects RBIP06LSS2 and RBLA032ZM7, and European Commission, contracts LSHB-CT-2005-019102 and LSHG-CT-2004-512077, are acknowledged.

Supporting Information Available: Crystallization and X-ray structure analysis, NMR data collection. This material is available free of charge via the Internet at <http://pubs.acs.org>.

References

- Brunger, A. T. X-ray crystallography and NMR reveal complementary views of structure and dynamics. *Nat. Struct. Biol.* **1997**, *4* (Suppl), 862–865.
- Medek, A.; Olejniczak, E. T.; Meadows, R. P.; Fesik, S. W. *J. Biomol. NMR* **2000**, *18*, 229.
- Bertini, I.; Calderone, V.; Fragai, M.; Giachetti, A.; Loconte, M.; Luchinat, C.; Maletta, M.; Nativi, C.; Yeo, K. J. Exploring the Subtleties of Drug–Receptor Interactions: The Case of Matrix Metalloproteinases. *J. Am. Chem. Soc.* **2007**, *129*, 2466–2475.
- Trzesniak, D.; Glättli, A.; Jaun, B.; Van Gunsteren, W. F. Interpreting NMR Data for beta-Peptides Using Molecular Dynamics Simulations. *J. Am. Chem. Soc.* **2005**, *127*, 14320–14329.
- Religa, T. L. Comparison of multiple crystal structures with NMR data for engrailed homeodomain. *J. Biomol. NMR* **2008**, *40*, 189–202.
- Trzesniak, D.; Van Gunsteren, W. F. Catalytic mechanism of cyclophilin as observed in molecular dynamics simulations: pathway prediction and reconciliation of X-ray crystallographic and NMR solution data. *Protein Sci.* **2006**, *15*, 2544–2551.
- Bonvin, A. M.; Brunger, A. T. Do NOE distance contain enough information to assess the relative populations of multiconformer structures. *J. Biomol. NMR* **1996**, *7*, 72–76.
- van Gunsteren, W. F.; Dolenc, J.; Mark, A. E. Molecular simulation as an aid to experimentalists. *Curr. Opin. Struct. Biol.* **2008**, *18*, 149–153.
- Vallurupalli, P.; Hansen, F.; Kay, L. E. Probing Structure in Invisible Protein States with Anisotropic NMR Chemical Shifts. *J. Am. Chem. Soc.* **2008**, *130*, 2734–2735.
- Vallurupalli, P.; Hansen, F.; Kay, L. E. Structures of invisible, excited protein states by relaxation dispersion NMR spectroscopy. *Proc. Natl. Acad. Sci. U.S.A.* **2008**, *105*, 11766–11771.
- Hansen, F.; Vallurupalli, P.; Lundström, P.; Neudecker, P.; Kay, L. E. Probing Chemical Shifts of Invisible States of Proteins with Relaxation Dispersion NMR Spectroscopy: How Well Can We Do? *J. Am. Chem. Soc.* **2008**, *130*, 2667–2675.
- Lindorff-Larsen, K.; Best, R. B.; DePristo, M. A.; Dobson, C. M.; Vendruscolo, M. Simultaneous determination of protein structure and dynamics. *Nature* **2005**, *433*, 128–132.
- Lange, O. F.; Lakomek, N. A.; Farès, C.; Schröder, G. F.; Walter, K. F.; Becker, S.; Meiler, J.; Grubmüller, H.; Griesinger, C.; de Groot, B. L. Recognition dynamics up to microseconds revealed from an RDC-derived ubiquitin ensemble in solution. *Science* **2008**, *321* (5882), 1429–1430.
- Zagrovic, B.; Jayachandran, G.; Millett, I. S.; Doniach, S.; Pande, V. S. How Large is an alpha-Helix? Studies of the Radii of Gyration of Helical Peptides by Small-Angle X-ray Scattering and Molecular Dynamics. *J. Mol. Biol.* **2005**, *353*, 232–241.
- Lau, A. Y.; Roux, B. The Free Energy Landscapes Governing Conformational Changes in a Glutamate Receptor Ligand-Binding Domain. *Structure* **2007**, *15*, 1203–1214.
- Bertini, I.; Fragai, M.; Giachetti, A.; Luchinat, C.; Maletta, M.; Parigi, G.; Yeo, K. J. Combining in Silico Tools and NMR Data to Validate Protein–Ligand Structural Models: Application to Matrix Metalloproteinases. *J. Med. Chem.* **2005**, *48*, 7544–7559.
- MacPherson, L. J.; Bayburt, E. K.; Capparelli, M. P.; Carroll, B. J.; Goldstein, R.; Justice, M. R.; Zhu, L.; Hu, S.-I.; Melton, R. A.; Fryer, L.; Goldberg, R. L.; Doughty, J. R.; Spirito, S.; Blancuzzi, V.; Wilson, D.; O'Byrne, E. M.; Ganu, V.; Parker, D. T. Discovery of CGS27023A, a Non-Peptidic, Potent, and Orally Active Stromelysin Inhibitor that Blocks Cartilage Degradation in Rabbits. *J. Med. Chem.* **1997**, *40* (16), 2525–2532.
- Mecham, R. P.; Broekelmann, T. J.; Fliszar, C. J.; Shapiro, S. D.; Welgus, H. G.; Senior, R. M. Elastin degradation by matrix metalloproteinases. Cleavage site specificity and mechanisms of elastolysis. *J. Biol. Chem.* **1997**, *272*, 18071–18076.
- Belaouaj, A.; Shipley, J. M.; Kobayashi, D. K.; Zimonjic, D. B.; Popescu, N.; Silverman, G. A.; Shapiro, S. D. Human macrophage metalloelastase. Genomic organization, chromosomal location, gene linkage, and tissue-specific expression. *J. Biol. Chem.* **1995**, *270*, 14568–14575.
- Vaalamo, M.; Karjalainen-Lindsberg, M. L.; Puolakkainen, P.; Kere, J.; Saarialho-Kere, U. Distinct expression profiles of stromelysin-2 (MMP-10), collagenase-3 (MMP-13), macrophage metalloelastase (MMP-12), and tissue inhibitor of metalloproteinases-3 (TIMP-3) in intestinal ulcerations. *Am. J. Pathol.* **1998**, *152*, 1005–1014.
- Hautamaki, R. D.; Kobayashi, D. K.; Senior, R. M.; Shapiro, S. D. Requirement for macrophage elastase for cigarette smoke-induced emphysema in mice. *Science* **1997**, *277*, 2002–2004.
- Shipley, J. M.; Wesselschmidt, R. L.; Kobayashi, D. K.; Ley, T. J.; Shapiro, S. D. Metalloelastase is required for macrophage-mediated proteolysis and matrix invasion in mice. *Proc. Natl. Acad. Sci. U.S.A.* **1996**, *93*, 942–946.
- Rosenberg, G. A. Matrix metalloproteinases and neuroinflammation in multiple sclerosis. *Neuroscientist* **2002**, *8*, 586–595.
- Snider, G. L. Understanding inflammation in chronic obstructive pulmonary disease: the process begins. *Am. J. Respir. Crit. Care Med.* **2003**, *167*, 1045–1046.
- Liu, M.; Sun, H.; Wang, X.; Koike, T.; Mishima, H.; Ikeda, K.; Watanabe, T.; Ochiai, N.; Fan, J. Association of increased expression of macrophage elastase (matrix metalloproteinase 12) with rheumatoid arthritis. *Arthritis Rheum.* **2004**, *50*, 3112–3117.
- Banci, L.; Bertini, I.; Ciulli, A.; Fragai, M.; Luchinat, C.; Terni, B. Expression and high yield production of the catalytic domain of matrix metalloproteinase 12 and of an active mutant with increased solubility. *J. Mol. Catal. A: Chem.* **2003**, *204–205*, 401–408.
- Lang, R.; Kocourek, A.; Braun, M.; Tschesche, H.; Huber, R.; Bode, W.; Maskos, K. Substrate specificity determinants of human macrophage elastase (MMP-12) based in the 1.1 Å crystal structure. *J. Mol. Biol.* **2001**, *312*, 731–742.
- Sethson, I.; Edlund, U.; Holak, T. A.; Ross, A.; Jonsson, B.-H. Sequential assignment of ^1H , ^{13}C , and ^{15}N resonances of human carbonic anhydrase I by triple-resonance NMR techniques and extensive amino acid specific ^{15}N labeling. *J. Biomol. NMR* **1996**, *8*, 417–428.
- Morales, R.; Perrier, S.; Florent, J. M.; Beltra, J.; Dufour, S.; De Mendez, I.; Manceau, P.; Tertre, A.; Moreau, F.; Compere, D.; Dublanchet, A. C.; O'Gara, M. Crystal structures of novel non-peptidic, non-zinc chelating inhibitors bound to MMP-12. *J. Mol. Biol.* **2004**, *341*, 1063–1076.
- McPherson, A., *Preparation and Analysis of Protein Crystals*; John Wiley: New York, 1982.
- Keller, R. *The Computer Aided Resonance Assignment Tutorial*, 1st ed.; Cantina Verlag: Goldau, Switzerland, 2004.
- Dewar, M. J. S.; Zebisch, E. G.; Healy, E. F.; Stewart, J. J. P. AM1: a new general purpose quantum mechanical molecular model. *J. Am. Chem. Soc.* **1985**, *107*, 3902–3909.
- Gasteiger, J.; Marsili, M. Iterative Partial Equilization of Orbital Electronegativity—A Rapid Access to Atomic Charges. *Tetrahedron* **1980**, *36*, 3219–3228.
- Kleywegt, G. J.; Jones, T. A. *Methods Enzymol.* **1997**, *277*, 208–230.
- Guha, R.; Howard, M. T.; Hutchinson, G. R.; Murray-Rust, P.; Rzepa, H.; Steinbeck, C.; Wegner, J. K.; Willighagen, E. The Blue Obelisk—Interoperability in Chemical Informatics. *J. Chem. Inf. Model.* **2006**, *46* (3), 991–998.
- MacKerell, A. D., Jr.; Wiórkiwicz-Kuczera, J.; Karplus, M. An All-Atom Empirical Energy Function for the Simulation of Nucleic Acids. *J. Am. Chem. Soc.* **1995**, *117*, 11946–11975.
- Best, R. B.; Lindorff-Larsen, K.; DePristo, M. A.; Vendruscolo, M. Relation between native ensembles and experimental structures of proteins. *Proc. Natl. Acad. Sci. U.S.A.* **2006**, *103* (29), 10901–10906.
- Nar, H.; Werle, K.; Bauer, M. M. T.; Dollinger, H.; Jung, B. Crystal Structure of Human Macrophage Elastase (MMP-12) in Complex with a Hydroxamic Acid Inhibitor. *J. Mol. Biol.* **2001**, *312*, 743–751.

- (39) Jones, T. A.; Zou, J. Y.; Cowan, S. W.; Kjeldgaard, M. Improved methods for building protein models in electron density maps and the location of errors in these models. *Acta Crystallogr., Sect. A: Found. Crystallogr.* **1991**, *47*, 110–119.
- (40) Gonella, N. C.; Li, Y.-C.; Zhang, X.; Paris, C. G. Bioactive Conformation of a Potent Stromelysin Inhibitor Determined by X-Nucleus Filtered and Multidimensional NMR Spectroscopy. *Bioorg. Med. Chem.* **1997**, *5* (12), 2193–2201.
- (41) Morris, G. M.; Goodsell, D. S.; Halliday, R. S.; Huey, R.; Hart, W. E.; Below, R. K.; Olson, A. J. Automated Docking Using a Lamarckian Genetic Algorithm and Empirical Binding Free Energy Function. *J. Comput. Chem.* **1998**, *19*, 1639–1662.
- (42) Schwieters, C. D.; Kuszewski, J. J.; Tjandra, N.; Clore, G. M. The Xplor-NIH NMR Molecular Structure Determination Package. *J. Magn. Reson.* **2003**, *160*, 66–74.
- (43) Bertini, I.; Calderone, V.; Cosenza, M.; Fragai, M.; Lee, Y.-M.; Luchinat, C.; Mangani, S.; Terni, B.; Turano, P. Conformational variability of matrix metalloproteinases: beyond a single 3D structure. *Proc. Natl. Acad. Sci. U.S.A.* **2005**, *102* (15), 5334–5339.
- (44) Rowsell, S.; Hawtin, P.; Minshull, C. A.; Jepson, H.; Brockbank, S. M.; Barratt, D. G.; Slater, A. M.; McPheat, W. L.; Waterson, D.; Henney, A. M.; Paupit, R. A. Crystal structure of human MMP9 in complex with a reverse hydroxamate inhibitor. *J. Mol. Biol.* **2002**, *319*, 173–181.
- (45) Tochowicz, A.; Maskos, K.; Huber, R.; Oltenfreiter, R.; Dive, V.; Yiotakis, A.; Zanda, M.; Bode, W.; Goettig, P. Crystal Structures of MMP-9 Complexes with Five Inhibitors: Contribution of the Flexible Arg424 Side Chain to Selectivity. *J. Mol. Biol.* **2007**, *371*, 989–1006.
- (46) Blagg, J. A.; Noe, M. C.; Wolf-Gouveia, L. A.; Reiter, L. A.; Laird, E. R.; Chang, S. P.; Danley, D. E.; Downs, J. T.; Elliott, N. C.; Eskra, J. D.; Griffiths, R. J.; Hardink, J. R.; Haugeto, A. I.; Jones, C. S.; Liras, J. L.; Lopresti-Morrow, L. L.; Mitchell, P. G.; Pandit, J.; Robinson, R. P.; Subramanyam, C.; Vaughn-Bowser, M. L.; Yocum, S. A. Potent pyrimidinetrione-based inhibitors of MMP-13 with enhanced selectivity over MMP-14. *Bioorg. Med. Chem. Lett.* **2005**, *15*, 1807–1810.
- (47) Wu, J.; Rush, T. S., III; Hotchandani, R.; Du, X.; Geck, M.; Collins, E.; Xu, Z. B.; Skotnicki, J.; Levin, J. I. Identification of potent and selective MMP-13 inhibitors. *Bioorg. Med. Chem. Lett.* **2005**, *15*, 4105–4109.
- (48) Johnson, A. R.; Pavlovsky, A. G.; Ortwine, D. F.; Prior, F.; Man, C. F.; Bornemeier, D. A.; Banotai, C. A.; Mueller, W. T.; McConnell, P.; Yan, C.; Baragi, V.; Lesch, C.; Roark, W. H.; Wilson, M.; Datta, K.; Guzman, R.; Han, H. K.; Dyer, R. D. Discovery and characterization of a novel inhibitor of matrix metalloproteinase-13 that reduces cartilage damage in vivo without joint fibroplasia side effects. *J. Biol. Chem.* **2007**, *282*, 27781–27791.
- (49) Li, J.; Brick, P.; O'Hare, M. C.; Skarzynski, T.; Lloyd, L. F.; Curry, V. A.; Clark, I. M.; Bigg, H. F.; Hazleman, B. L.; Cawston, T. E. Structure of full-length porcine synovial collagenase reveals a C-terminal domain containing a calcium-linked, four-bladed beta-propeller. *Structure* **1995**, *3*, 541–549.

JM801388Q